4'-Functionalized 2,2':6',2''-terpyridines as the N^N domain in $[Ir(C^N)_2(N^N)][PF_6]$ complexes†

Daniel P. Ris, Gabriel E. Schneider, Cathrin D. Ertl, Emanuel Kohler, Thomas Müntener, Markus Neuburger, Edwin C. Constable,* and Catherine E. Housecroft*

Department of Chemistry, University of Basel, Spitalstrasse 51, 4056 Basel, Switzerland

E-mail: catherine.housecroft@unibas.ch

†This paper is dedicated to the memory of Jack Lewis in recognition of his lifelong contributions to science and his personal mentoring.

Abstract

The cyclometallated iridium(III) complexes $[Ir(ppy)_2(N^N)][PF_6]$ (Hppy = 2-phenylpyridine) with N^N = 4'-chloro-2,2':6',2''-terpyridine (**1**), 4'-methoxy-2,2':6',2''-terpyridine (**2**), 4'-ethoxy-2,2':6',2''-terpyridine (**3**), 4'-methylthio-2,2':6',2''-terpyridine (**4**), 4'-phenylthio-2,2':6',2''-terpyridine (**5**) and 4'-dimethylamino-2,2':6',2''-terpyridine (**6**) are reported including the single crystal structures of $2\{[Ir(ppy)_2(\mathbf{1})][PF_6]\}\cdot 0.6Et_2O\cdot CH_2Cl_2$, $[Ir(ppy)_2(\mathbf{5})][PF_6]\cdot 0.5CH_2Cl_2$ and $[Ir(ppy)_2(\mathbf{6})][PF_6]$. The single crystal structure of $[Ir(ppy)_2(\mathbf{3})]Cl\cdot 2H_2O\cdot MeCN$ is also reported. In each complex, the 2,2':6',2''-terpyridine (tpy) ligand binds to the metal centre in a bidentate fashion with the non-coordinated pyridine ring folded into the coordination sphere and engaging in a pyridine–phenyl π-stacking interaction. Solution NMR spectra are consistent with hindered rotation of the non-coordinated pyridine ring at 298 K, with intra-cation CH...N(pyridine) hydrogen bond formation between adjacent

[ppy]$^-$ and tpy ligands. Trends in the electrochemical HOMO–LUMO gaps and emission maxima of the complexes (in CH_2Cl_2 solution) are consistent with the electron-withdrawing or releasing properties of the 4'-tpy substituent; in degassed solution, [Ir(ppy)$_2$(**6**)][PF_6] has a quantum yield of 24.8% and emission lifetime of 441 ns, while the other complexes exhibit significantly lower quantum yields and shorter lifetimes.

Keywords: Cyclometallated iridium(III) complexes; 2,2':6',2"-terpyridine; photoluminescence; crystal structure; electrochemistry

1. Introduction

Manipulating the emissive behaviour of [Ir(C^N)$_2$(N^N)][PF_6] complexes in which C^N is a cyclometallated ligand and N^N an *N,N*'-chelating ligand is of importance for their successful application in light-emitting electrochemical cells (LECs). Colour tuning is now well developed by using substituent effects in either or both of the C^N and N^N domains [1]. This structure-property modulation is predicated upon the localization of HOMO character on the iridium centre and cyclometallated ligands, and the LUMO on the N^N domain. In addition to tuning of emission colours for LECs, extending the lifetime of the device is essential. One strategy that we have exploited in [Ir(C^N)$_2$(N^N)]$^+$ complexes is to protect the iridium centre in the excited state from attack, e.g. by water, through the use of π-stacked interactions between an aryl substituent in the N^N and the phenyl ring in one C^N ligand [2-14]. This has led to remarkably long-lived LEC devices with lifetimes exceeding 2500 hours [15]. Similar π-stacking interactions between pendant aromatic units and coordinated C^N ligands have been exploited to tune the photophysical properties of [Ir(C^N)$_2$(N^N)]$^+$ complexes bearing lanthanoid-containing domains linked through the N^N ligand [16,17].

Although we have favoured phenyl substituents (e.g. 6-phenyl-2,2'-bipyridine) for formation of intramolecular π-stacking in $[Ir(C^N)_2(N^N)][PF_6]$ complexes, we have also shown that 2,2':6',2''-terpyridine (tpy) binds in a bidentate mode in $[Ir(C^N)_2(tpy)]^+$ with the non-coordinated pyridine ring π-stacked over an adjacent cyclometallated ligand [18]. We now extend this study to a series of $[Ir(ppy)_2(N^N)][PF_6]$ complexes in which N^N is a 4'-substituted tpy (Scheme 1). The substituents have been chosen to include electron-withdrawing and donating groups, and we illustrate the effects of a remote substituent on the emission behaviour of the complexes.

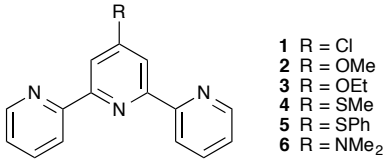

Scheme 1. Structures of the N^N ligands.

2. Experimental

2.1 General

A Biotage Initiator 8 reactor was used for syntheses under microwave conditions. ^1H and ^{13}C NMR spectra were recorded on a Bruker DRX-500 NMR spectrometer (295 K unless otherwise stated) with chemical shifts referenced to residual solvent peaks (∂(TMS) = 0 ppm). Solution electronic absorption and emission spectra were recorded on an Agilent 8453 spectrophotometer and Shimadzu RF-5301 PC spectrofluorometer, respectively, and FT-IR spectra on a Shimadzu 8400S instrument with Golden Gate accessory. Solution quantum yields were measured using a Hamamatsu absolute PL quantum yield spectrometer C11347 Quantaurus-QY. Lifetimes were measured using a Hamamatsu Compact Fluorescence lifetime Spectrometer C11367 Quantaurus-Tau. Electrospray ionization (ESI) mass spectra were recorded using a Bruker esquire 3000^{plus} mass spectrometer.

Electrochemical measurements were performed on a CHI 900B instrument. A glassy carbon working electrode, platinum wire auxiliary electrode, and a silver wire pseudo-reference electrode were used. Potentials were determined by both cyclic voltammetery (CV) and square wave voltammetry. HPLC grade, argon degassed CH_2Cl_2 solutions ($\approx 10^{-4}$ mol dm^{-3}) of the samples were measured in the presence of 0.1 M [$^nBu_4N$][PF_6] as supporting electrolyte; the scan rate was 0.1 V s^{-1} and ferrocene was used as an internal standard, added at the end of each experiment.

$[Ir_2(ppy)_4Cl_2]$ [19] and compounds **1** [20], **2** [21], **3** [21], **4** [22], **5** [23] and **6** [23] were prepared according to literature procedures.

*2.2 [Ir(ppy)$_2$(**1**)][PF$_6$]*

A microwave vial was charged with $[Ir(ppy)_2(\mu\text{-}Cl)]_2$ (107 mg, 0.100 mmol) and **1** (53.5 mg, 0.200 mmol) and then MeOH (15 mL) was added. The yellow suspension was heated to 120°C for 2 h (P = 13 bar) in a microwave reactor. An orange solution was obtained and excess NH_4PF_6 (326 mg, 2.00 mmol) and $AgPF_6$ (50.6 mg, 0.200 mmol) was added under stirring. An orange precipitate formed and the solvent was removed under reduced pressure. The yellow solid was subjected to flash chromatography (SiO_2, CH_2Cl_2 changing to CH_2Cl_2/MeOH 98:2). After removing the solvent under reduced pressure, $[Ir(ppy)_2(\mathbf{1})][PF_6]$ was obtained as an orange solid (167 mg, 0.183 mmol, 91%). ^{1}H NMR (500 MHz, CD_2Cl_2) δ/ppm: 8.91 (d, J = 1.8 Hz, 1H, H^{F3}), 8.90 (br, 1H, H^{B6}), 8.72 (dt, J = 8.4, 1.0 Hz, 1H, H^{E3}), 8.23 (dt, J = 4.9, 1.4 Hz, 1H, H^{G6}), 8.16 (td, J = 8.0, 1.6 Hz, 1H, H^{E4}), 7.90 (dt, J = 8.3, 1.2 Hz, 1H, H^{B3}), 7.86 (dt, J = 8.4, 0.9 Hz, 1H, H^{D3}), 7.85-7.79 (m, 3H, $H^{B4+D4+E6}$), 7.62 (dd, J = 8.0, 1.4 Hz, 1H, H^{A3}), 7.44 (d, J = 2.1 Hz, 1H, H^{F5}), 7.42 (m, 1H, H^{E5}), 7.38 (dt, J = 5.9, 1.2 Hz, 1H, H^{D6}), 7.35 (dd, J = 7.8, 1.3 Hz, 1H, H^{C3}), 7.17 (m, 1H, H^{B5}), 7.14 (td, J = 7.9, 1.9 Hz, 1H, H^{G4}), 7.01 (m, 1H, H^{D5}), 6.96 (m, 2H, H^{A4+G5}), 6.76 (m, 1H, H^{A5}), 6.64 (td, J = 7.4, 1.2 Hz, 1H, H^{C4}), 6.54

(d, J = 7.7 Hz, 1H, H^{G3}), 6.33 (td, J = 7.4, 1.3 Hz, 1H, H^{C5}), 5.87 (dd, J = 7.8, 1.2 Hz, 1H, H^{A6}), 5.44 (dd, J = 7.7, 1.1 Hz, 1H, H^{C6}). $^{13}C\{^1H\}$ NMR (126 MHz, CD_2Cl_2) δ/ppm: 168.6 (C^{D2}), 166.9 (C^{B2}), 164.1 (C^{F6}), 158.9 (C^{F2}), 156.1 (C^{E2}), 155.2 (C^{G2}), 152.8 (C^{B6}), 151.0 (C^{E6}), 149.9 (C^{C1}), 148.8 (C^{G6}), 148.4 (C^{D6+F4}), 146.1 (C^{A1}), 143.5 (C^{A2}), 142.8 (C^{C2}), 140.0 (C^{E4}), 138.9 (C^{D4}), 138.7 (C^{B4}), 136.9 (C^{G4}), 132.9 (C^{C6}), 131.02 (C^{A6}), 130.96 (C^{A5}), 130.5 (C^{C5}), 129.4 (C^{F5}), 128.8 (C^{E5}), 126.1 (C^{E3}), 125.2 (C^{A3}), 125.0 (C^{G5}), 124.8 (C^{F3}), 124.3 (C^{C3}), 123.4 (3C, $C^{B5+D5+A4}$), 123.1 (C^{G3}), 121.4 (C^{C4}), 120.0 (C^{D3}), 119.9 (C^{B3}). ESI MS *m/z*: 768.2 $[M–PF_6]^+$ (calcd. 768.2). UV-Vis (CH_2Cl_2, 1.25 × 10^{-5} M) λ/nm (ε/dm^3 mol^{-1} cm^{-1}): 262 (51700), 310sh (29000), 385sh (7600). Found C 46.43, H 2.94, N 7.45; $C_{37}H_{26}ClF_6IrN_5P·2H_2O$ requires C 46.81, H 3.19, N 7.38%.

*2.3 [Ir(ppy)$_2$(**2**)][PF$_6$]*

The method was as for [Ir(ppy)$_2$(**1**)][PF$_6$] starting with [Ir(ppy)$_2$(μ-Cl)]$_2$ (107 mg, 0.100 mmol) and **2** (54 mg, 0.200 mmol) in MeOH (15 mL). After anion exchange with NH_4PF_6 (326 mg, 2.00 mmol) and $AgPF_6$ (50.6 mg, 0.200 mmol), [Ir(ppy)$_2$(**2**)][PF$_6$] was obtained as an orange solid (166 mg, 0.183 mmol, 92%). ^1H NMR (500 MHz, CD_2Cl_2) δ/ppm: 8.82 (br, 1H, H^{B6}), 8.51 (d, J = 8.2 Hz, 1H, H^{E3}), 8.19 (d, J = 4.6 Hz, 1H, H^{G6}), 8.16 (td, J = 8.0, 1.6 Hz, 1H, H^{E4}), 7.98 (d, J = 2.6 Hz, 1H, H^{F3}), 7.87 (m, 2H, H^{B3+D3}), 7.80 (m, 3H, $H^{B4+D4+E6}$), 7.60 (dd, J = 7.8, 1.2 Hz, 1H, H^{A3}), 7.44 (d, J = 7.8 Hz, 1H, H^{D6}), 7.35 (m, 2H, H^{E5+C3}), 7.16 (m, 1H, H^{B5}), 7.12 (t, J = 7.4 Hz, 1H, H^{G4}), 6.99 (m, 1H, H^{D5}), 6.97-6.91 (m, 3H, $H^{A4+F5+G5}$), 6.76 (td, J = 7.5, 1.3 Hz, 1H, H^{A5}), 6.63 (td, J = 7.6, 1.2 Hz, 1H, H^{C4}), 6.51 (d, J = 7.5 Hz, 1H, H^{G3}), 6.33 (td, J = 7.5, 1.3 Hz, 1H, H^{C5}), 5.90 (dd, J = 7.8, 0.8 Hz, 1H, H^{A6}), 5.46 (d, J = 7.1 Hz, 1H, H^{C6}), 4.06 (s, 3H, H^{OMe}). $^{13}C\{^1H\}$ NMR (126 MHz, CD_2Cl_2) δ/ppm: 168.7 (C^{D2}), 168.4 (C^{F4}), 167.1 (C^{B2}), 164.5 (C^{F6}), 159.1 (C^{F2}), 157.3 (C^{E2}), 155.9 (C^{G2}), 152.6 (C^{B6}), 150.7 (C^{E6}), 150.6 (C^{C1}), 148.6 (C^{D6}), 148.3 (C^{G6}), 147.1 (C^{A1}), 143.7 (C^{A2}), 142.9 (C^{C2}), 139.7 (C^{E4}), 138.6 (C^{D4}),

138.5 (C^{B4}), 137.0 (C^{G4}), 132.8 (C^{C6}), 131.1 (C^{A6}), 130.9 (C^{A5}), 130.4 (C^{C5}), 128.2 (C^{E5}), 125.7 (C^{E3}), 125.1 (C^{A3}), 124.8 (C^{G5}), 124.4 (C^{C3}), 123.4 (C^{B5}), 123.2 ($C^{G3+A4+D5}$), 121.2 (C^{C4}), 119.9 (C^{D3}), 119.8 (C^{B3}), 115.0 (C^{F5}), 111.4 (C^{F3}), 57.4 (C^{OMe}). ESI MS *m/z*: 764.2 $[M–PF_6]^+$ (calcd. 764.2). UV-Vis (CH_2Cl_2, 1.25 × 10^{-5} M) λ/nm (ε/dm^3 mol^{-1} cm^{-1}): 262 (53200), 307sh (26700), 379sh (6800). Found C 49.30, H 3.62, N 7.66; $C_{38}H_{29}F_6IrN_5OP·H_2O$ requires C 49.24, H 3.37, N 7.56%.

*2.4 [Ir(ppy)$_2$(**3**)][PF$_6$]*

The method was as for [Ir(ppy)$_2$(**1**)][PF_6] starting with [Ir(ppy)$_2$(μ-Cl)]$_2$ (107 mg, 0.100 mmol) and **3** (55.5 mg, 0.200 mmol) in EtOH (15 mL). After anion exchange using NH_4PF_6 (163 mg, 1.00 mmol) and $AgPF_6$ (50.6 mg, 0.200 mmol), the product was purified by flash chromatography (SiO_2, CH_2Cl_2 changing to CH_2Cl_2/MeOH 97:3). After removing the solvent under reduced pressure, the residue was dissolved in CH_2Cl_2 and precipitated with Et_2O to obtain [Ir(ppy)$_2$(**3**)][PF_6] as a yellow solid (118 mg, 0.128 mmol, 64%). ^{1}H NMR (500 MHz, CD_2Cl_2) δ/ppm: 8.85 (br, 1H, H^{B6}), 8.49 (dt, *J* = 8.3, 1.0 Hz, 1H, H^{E3}), 8.18 (dt, *J* = 4.8, 1.4 Hz, 1H, H^{G6}), 8.12 (td, *J* = 7.9, 1.7 Hz, 1H, H^{E4}), 7.95 (d, *J* = 2.6 Hz, 1H, H^{F3}), 7.88-7.84 (m, 2H, H^{B3+D3}), 7.82-7.76 (m, 3H, $H^{B4+D4+E6}$), 7.61 (dd, *J* = 7.8, 1.4 Hz, 1H, H^{A3}), 7.43 (dt, *J* = 5.8, 1.1 Hz, 1H, H^{D6}), 7.37-7.33 (m, 2H, H^{E5+C3}), 7.15 (m, 1H, H^{B5}), 7.09 (td, *J* = 7.7, 1.7 Hz, 1H, H^{G4}), 6.99 (m, 1H, H^{D5}), 6.96 (td, *J* = 7.7, 1.2 Hz, 1H, H^{A4}), 6.89 (m, 2H, H^{F5+G5}), 6.75 (td, *J* = 7.5, 1.4 Hz, 1H, H^{A5}), 6.62 (td, *J* = 7.5, 1.2 Hz, 1H, H^{C4}), 6.48 (d, *J* = 7.7 Hz, 1H, H^{G3}), 6.32 (td, *J* = 7.4, 1.3 Hz, 1H, H^{C5}), 5.90 (dd, *J* = 7.7, 1.2 Hz, 1H, H^{A6}), 5.45 (d, *J* = 7.7, 1.1 Hz, 1H, H^{C6}), 4.30 (q, *J* = 7.0 Hz, 2H, H^{OCH_2Me}), 1.48 (t, *J* = 7.0 Hz, 3H, H^{OCH_2Me}). $^{13}C\{^1H\}$ NMR (126 MHz, CD_2Cl_2) δ/ppm: 168.8 (C^{D2}), 167.7 (C^{F4}), 167.2 (C^{B2}), 164.8 (C^{F6}), 159.0 (C^{F2}), 157.4 (C^{E2}), 156.3 (C^{G2}), 152.7 (C^{B6}), 150.7 (C^{E6}), 150.6 (C^{C1}), 148.6 (C^{G6}), 148.5 (C^{D6}), 147.2 (C^{A1}), 143.8 (C^{A2}), 142.9 (C^{C2}), 139.7 (C^{E4}), 138.6 (C^{D4}), 138.5 (C^{B4}), 136.7

(C^{G4}), 132.8 (C^{C6}), 131.2 (C^{A6}), 130.9 (C^{A5}), 130.4 (C^{C5}), 128.2 (C^{E5}), 125.6 (C^{E3}), 125.1 (C^{A3}), 124.6 (C^{G5}), 124.3 (C^{C3}), 123.3 (C^{B5}), 123.1 (C^{A4+D5}), 123.0 (C^{G3}), 121.2 (C^{C4}), 119.9 (C^{D3}), 119.8 (C^{B3}), 115.2 (C^{F5}), 111.6 (C^{F3}), 66.4 (C^{OCH_2Me}), 14.6 ($C^{OCH_2\mathit{Me}}$). ESI MS *m/z*: 778.2 $[M–PF_6]^+$ (calcd. 778.2). UV-Vis (CH_2Cl_2, 1.25 × 10^{-5} M) λ/nm (ε/dm^3 mol^{-1} cm^{-1}): 262 (54700), 307sh (26700), 379sh (6800). Found C 50.52, H 3.90, N 7.05; $C_{39}H_{31}F_6IrN_5OP·0.5H_2O$ requires C 50.27, H 3.46, N 7.52%.

*2.5 [Ir(ppy)$_2$(**4**)][PF$_6$]*

The method was as for [Ir(ppy)$_2$(**1**)][PF$_6$] starting with [Ir(ppy)$_2$(μ-Cl)]$_2$ (150 mg, 0.14 mmol) and **4** (78.2 mg, 0.280 mmol) in MeOH (15 mL). After anion exchange with excess aqueous NH_4PF_6, the precipitate that formed was filtered, washed with water and subjected to flash chromatography (Al_2O_3, CH_2Cl_2 changing to CH_2Cl_2/MeOH 99.5:0.5). After removing the solvent under reduced pressure, [Ir(ppy)$_2$(**4**)][PF$_6$] was obtained as an orange solid (192 mg, 0.246 mmol, 74%). ^{1}H NMR (500 MHz, CD_2Cl_2) δ/ppm: 8.88 (br, 1H, H^{B6}), 8.52 (dt, *J* = 8.3, 1.1 Hz, 1H, H^{E3}), 8.22 (d, *J* = 2.0 Hz, 1H, H^{F3}), 8.20 (dt, *J* = 4.9, 1.3 Hz, 1H, H^{G6}), 8.14 (td, *J* = 7.9, 1.7 Hz, 1H, H^{E4}), 7.89-7.85 (m, 2H, H^{B3+D3}), 7.83-7.77 (m, 3H, $H^{B4+D4+E6}$), 7.61 (dd, *J* = 7.8, 1.4 Hz, 1H, H^{A3}), 7.44 (dt, *J* = 5.8, 1.2 Hz, 1H, H^{D6}), 7.38-7.34 (m, 2H, H^{E5+C3}), 7.17-7.14 (m, 2H, H^{B5+F5}), 7.09 (td, *J* = 7.7, 1.7 Hz, 1H, H^{G4}), 7.00 (ddd, *J* = 7.3, 5.8, 1.6 Hz, 1H, H^{D5}), 6.95 (td, *J* = 7.5, 1.2 Hz, 1H, H^{A4}), 6.91 (m, 1H, H^{G5}), 6.76 (td, *J* = 7.5, 1.4 Hz, 1H, H^{A5}), 6.63 (td, *J* = 7.5, 1.2 Hz, 1H, H^{C4}), 6.49 (d, *J* = 7.7 Hz, 1H, H^{G3}), 6.32 (td, *J* = 7.4, 1.3 Hz, 1H, H^{C5}), 5.89 (dd, *J* = 7.7, 1.2 Hz, 1H, H^{A6}), 5.44 (dd, *J* = 7.6, 1.2 Hz, 1H, H^{C6}), 2.64 (s, 3H, $H^{S\mathit{Me}}$). $^{13}C\{^1H\}$ NMR (126 MHz, CD_2Cl_2) δ/ppm: 168.7 (C^{D2}), 167.1 (C^{B2}), 162.0 (C^{F6}), 157.0 (C^{F4+E2}), 156.5 (C^{F2}), 156.2 (C^{G2}), 152.7 (C^{B6}), 150.8 (C^{E6}), 150.5 (C^{C1}), 148.7 (C^{G6}), 148.4 (C^{D6}), 147.2 (C^{A1}), 143.7 (C^{A2}), 142.8 (C^{C2}), 139.8 (C^{E4}), 138.6 (C^{D4}), 138.5 (C^{B4}), 136.6 (C^{G4}), 132.8 (C^{C6}), 131.1 (C^{A6}), 130.9 (C^{A5}), 130.4 (C^{C5}), 128.2 (C^{E5}), 125.7 (C^{E3}), 125.1

(C^{A3}), 124.7 (C^{G5}), 124.29 (C^{C3}), 124.25 (C^{F5}), 123.3 (C^{B5}), 123.2 (C^{A4+D5}), 123.0 (C^{G3}), 121.2 (C^{C4}), 120.0 (C^{F3}), 119.9 (C^{D3}), 119.8 (C^{B3}), 14.5 (C^{SMe}). ESI MS *m/z*: 780.2 [M–PF_6]$^+$ (calcd. 780.2). UV-Vis (CH_2Cl_2, 1.25 × 10^{-5} M) λ/nm (ε/dm^3 mol^{-1} cm^{-1}): 272 (57400), 293sh (46400), 383sh (9100). Found C 48.54, H 3.48, N 7.61; $C_{38}H_{29}F_6IrN_5PS \cdot H_2O$ requires C 48.40, H 3.31, N 7.43%.

*2.6 [Ir(ppy)$_2$(**5**)][PF$_6$]*

The method was as for [Ir(ppy)$_2$(**1**)][PF_6] starting with [Ir(ppy)$_2$(μ-Cl)]$_2$ (107 mg, 0.100 mmol) and **5** (68.3 mg, 0.200 mmol) in MeOH (15 mL). After ion exchange with NH_4PF_6 (326 mg, 2.00 mmol) and $AgPF_6$ (50.6 mg, 0.200 mmol), the product was purified using flash chromatography (SiO_2, CH_2Cl_2 changing to CH_2Cl_2/MeOH 98:2). After removing the solvent under reduced pressure, [Ir(ppy)$_2$(**5**)][PF_6] was isolated as an orange solid (187 mg, 0.189 mmol, 95%). ^{1}H NMR (500 MHz, CD_2Cl_2) δ/ppm: 8.82 (br, 1H, H^{B6}), 8.15 (m, 2H, H^{G6+E3}), 8.07 (td, *J* = 7.9, 1.6 Hz, 1H, H^{E4}), 7.98 (d, *J* = 2.0 Hz, 1H, H^{F3}), 7.86 (m, 2H, H^{B3+D3}), 7.82 (m, 2H, H^{B4+D4}), 7.76 (ddd, *J* = 5.5, 1.7, 0.8 Hz, 1H, H^{E6}), 7.65-7.63 (m, 2H, H^{H2}), 7.60 (dd, *J* = 7.9, 1.4 Hz, 1H, H^{A3}), 7.55 (m, 3H, H^{H3+H4}), 7.38 (dt, *J* = 5.7, 1.1 Hz, 1H, H^{D6}), 7.34 (m, 2H, H^{E5+C3}), 7.16 (m, 1H, H^{B5}), 7.04 (td, *J* = 7.7, 1.8 Hz, 1H, H^{G4}), 7.01 (m, 1H, H^{D5}), 6.97-6.94 (m, 2H, H^{F5+A4}), 6.87 (m, 1H, H^{G5}), 6.75 (td, *J* = 7.5, 1.3 Hz, 1H, H^{A5}), 6.61 (td, *J* = 7.5, 1.2 Hz, 1H, H^{C4}), 6.40 (d, *J* = 7.7 Hz, 1H, H^{G3}), 6.31 (td, *J* = 7.5, 1.3 Hz, 1H, H^{C5}), 5.87 (d, *J* = 7.8 Hz, 1H, H^{A6}), 5.42 (dd, *J* = 7.7, 1.2 Hz, 1H, H^{C6}). ^{13}C{^{1}H} NMR (126 MHz, CD_2Cl_2) δ/ppm: 168.7 (C^{D2}), 167.0 (C^{B2}), 162.4 (C^{F6}), 157.2 (C^{F4}), 156.8 (C^{E2}), 156.75 (C^{F2}), 155.9 (C^{G2}), 152.6 (C^{B6}), 150.9 (C^{E6}), 150.3 (C^{C1}), 148.6 (C^{G6}), 148.5 (C^{D6}), 146.9 (C^{A1}), 143.6 (C^{A2}), 142.8 (C^{C2}), 139.7 (C^{E4}), 138.7 (C^{D4}), 138.6 (C^{B4}), 136.7 (C^{G4}), 136.0 (C^{H2}), 132.7 (C^{C6}), 131.6 (C^{H4}), 131.2 (C^{H3}), 131.0 (C^{A6}), 130.9 (C^{A5}), 130.4 (C^{C5}), 128.4 (C^{E5}), 127.2 (C^{H1}), 125.3 (C^{E3}), 125.1 (C^{A3}), 124.8 (C^{G5}), 124.7 (C^{F5}), 124.3 (C^{C3}),

123.34 (C^{B5}), 123.25 (C^{A4}), 123.2 (C^{D5}), 123.0 (C^{G3}), 121.2 (C^{C4}), 120.1 (C^{F3}), 120.0 (C^{D3}), 119.8 (C^{B3}). ESI MS *m/z*: 842.2 $[M–PF_6]^+$ (calcd. 842.2). UV-Vis (CH_2Cl_2, 1.25 × 10^{-5} M) λ/nm (ε/dm^3 mol^{-1} cm^{-1}): 269 (57000), 293sh (48200), 384sh (9400). Found C 51.22, H 3.45, N 7.10; $C_{43}H_{31}F_6IrN_5PS·H_2O$ requires C 51.39, H 3.31, N 6.97%.

*2.7 [Ir(ppy)$_2$(**6**)][PF$_6$]*

The method was as for $[Ir(ppy)_2(\mathbf{1})][PF_6]$ starting with $[Ir(ppy)_2(\mu\text{-}Cl)]_2$ (107 mg, 0.100 mmol) and **6** (55.3 mg, 0.200 mmol) in MeOH (15 mL). After anion exchange using NH_4PF_6 (326 mg, 2.00 mmol) and $AgPF_6$ (50.6 mg, 0.200 mmol) and workup as for $[Ir(ppy)_2(\mathbf{1})][PF_6]$, the complex $[Ir(ppy)_2(\mathbf{6})][PF_6]$ was obtained as an orange solid (180 mg, 0.195 mmol, 98%). ^{1}H NMR (500 MHz, CD_2Cl_2) δ/ppm: 8.82 (br, 1H, H^{B6}), 8.48 (dt, *J* = 8.4, 1.1 Hz, 1H, H^{E3}), 8.14 (dt, *J* = 4.9, 1.4 Hz, 1H, H^{G6}), 8.08 (td, *J* = 7.9, 1.7 Hz, 1H, H^{E4}), 7.85 (m, 2H, H^{B3+D3}), 7.81-7.74 (m, 3H, $H^{B4+D4+E6}$), 7.59 (dd, *J* = 7.9, 1.4 Hz, 1H, H^{A3}), 7.56 (d, *J* = 2.8 Hz, 1H, H^{F3}), 7.50 (dt, *J* = 5.9, 1.1 Hz, 1H, H^{D6}), 7.34 (dd, *J* = 8.0, 1.3 Hz, 1H, H^{C3}), 7.30 (m, 1H, H^{E5}), 7.15 (m, 1H, H^{B5}), 7.05 (td, *J* = 7.7, 1.8 Hz, 1H, H^{G4}), 6.99 (m, 1H, H^{D5}), 6.94 (td, *J* = 7.5, 1.2 Hz, 1H, H^{A4}), 6.87 (m, 1H, H^{G5}), 6.75 (td, *J* = 7.4, 1.2 Hz, 1H, H^{A5}), 6.61 (td, *J* = 7.7, 1.2 Hz, 1H, H^{C4}), 6.50 (d, *J* = 2.8 Hz, 1H, H^{F5}), 6.43 (d, *J* = 7.8 Hz, 1H, H^{G3}), 6.31 (td, *J* = 7.4, 1.3 Hz, 1H, H^{C5}), 5.93 (dd, *J* = 7.8, 1.2 Hz, 1H, H^{A6}), 5.46 (d, *J* = 7.6, 1.2 Hz, 1H, H^{C6}), 3.19 (s, 6H, H^{NMe_2}). ^{13}C{^{1}H} NMR (126 MHz, CD_2Cl_2) δ/ppm: 168.8 (C^{D2}), 167.4 (C^{B2}), 162.5 (C^{F6}), 158.5 (C^{E2}), 157.1 (C^{G2}), 157.0 (C^{F2}), 155.4 (C^{F4}), 152.5 (C^{B6}), 151.3 (C^{C1}), 150.5 (C^{E6}), 148.64 (C^{D6}), 148.56 (C^{A1}), 148.2 (C^{G6}), 144.0 (C^{A2}), 142.9 (C^{C2}), 139.3 (C^{E4}), 138.2 (C^{B4+D4}), 136.5 (C^{G4}), 132.6 (C^{C6}), 131.2 (C^{A6}), 130.8 (C^{A5}), 130.2 (C^{C5}), 127.5 (C^{E5}), 125.0 (C^{E3+A3}), 124.3 (C^{C3}), 124.2 (C^{G5}), 123.2 (C^{B5}), 123.1 (C^{G3}), 122.9 (C^{A4+D5}), 120.9 (C^{C4}), 119.7 (C^{D3}), 119.6 (C^{B3}), 110.8 (C^{F5}), 107.1 (C^{F3}), 40.0 (C^{NMe_2}). ESI MS *m/z*: 777.2 $[M–PF_6]^+$ (calcd. 777.2). UV-Vis (CH_2Cl_2, 1.25 × 10^{-5} M) λ/nm (ε/dm^3 mol^{-1} cm^{-1}): 273

(61100), 292sh (44100), 380sh (9300). Found C 49.64, H 3.63, N 9.03; $C_{39}H_{32}F_6IrN_6P \cdot H_2O$ requires C 49.84, H 3.65, N 8.94%.

2.7 Crystal structure determinations

Data were collected on a Bruker Kappa Apex2 diffractometer with data reduction, solution and refinement using the programs APEX [24] and CRYSTALS [25]. The program Mercury v. 3.5.1 [26, 27] was used for structural analysis and for drawing ORTEP-style figures.

*2.8 2{[Ir(ppy)$_2$(**1**)][PF$_6$]}·0.6Et$_2$O·CH$_2$Cl$_2$*

$C_{74}H_{52}Cl_2F_{12}Ir_2N_{10}O_2P_2$, M = 1955.97, orange block, monoclinic, space group Cc, a = 20.2992(11), b = 15.4325(11), c = 24.1481(16) Å, β = 99.833(5)°, U = 7453.7(8) Å^3, Z = 4, D_c = 1.743 Mg m^{-3}, μ(Mo-Kα) = 3.837 mm^{-1}, T = 123 K. Total 90182 reflections, 26730 unique, R_{int} = 0.047. Refinement of 22115 reflections (992 parameters) with I >2σ (I) converged at final $R1$ = 0.0336 ($R1$ all data = 0.0461), $wR2$ = 0.0346 ($wR2$ all data = 0.0500), gof = 1.0196.

*2.9 [Ir(ppy)$_2$(**3**)]Cl·2H$_2$O·MeCN*

$C_{41}H_{38}ClIrN_6O_3$, M = 890.46, yellow plate, monoclinic, space group $P2_1/c$, a = 12.8163(8), b = 34.786(2), c = 8.2433(6) Å, β = 95.167(3)°, U = 3660.2(4) Å^3, Z = 4, D_c = 1.616 Mg m^{-3}, μ(Mo-Kα) = 3.769 mm^{-1}, T = 123 K. Total 93367 reflections, 13234 unique, R_{int} = 0.062. Refinement of 10257 reflections (469 parameters) with I >2σ (I) converged at final $R1$ = 0.0277 ($R1$ all data = 0.0404), $wR2$ = 0.0299 ($wR2$ all data = 0.0344), gof = 1.0655.

*2.10 [Ir(ppy)$_2$(**5**)][PF$_6$]·0.5CH$_2$Cl$_2$*

$C_{43.5}H_{32}ClF_6IrN_5PS$, M = 1029.47, orange block, triclinic, space group P–1, a = 11.8012(6), b = 18.5920(10), c = 19.0690(10) Å, α = 80.025(2), β = 85.496(2), γ = 84.315(2)°, U = 4092.3(4) Å^3, Z = 4, D_c = 1.671 Mg m^{-3}, μ(Cu-Kα) = 8.335 mm^{-1}, T = 123 K. Total 71659 reflections, 14638 unique, R_{int} = 0.031. Refinement of 13991 reflections (1354 parameters) with I >2σ (I) converged at final R1 = 0.0368 (R1 all data = 0.0383), wR2 = 0.0404 (wR2 all data = 0.0444), gof = 1.1465.

*2.11 [Ir(ppy)$_2$(**6**)][PF$_6$]*

$C_{39}H_{32}F_6IrN_6P$, M = 921.90, yellow block, monoclinic, space group $P2_1/c$, a = 15.3927(8), b = 13.6629(7), c = 17.9681(10) Å, β = 110.042(2)°, U = 3550.0(3) Å^3, Z = 4, D_c = 1.725 Mg m^{-3}, μ(Cu-Kα) = 8.319 mm^{-1}, T = 123 K. Total 34390 reflections, 6432 unique, R_{int} = 0.026. Refinement of 6400 reflections (478 parameters) with I >2σ (I) converged at final R1 = 0.0213 (R1 all data = 0.0213), wR2 = 0.0221 (wR2 all data = 0.0221), gof = 1.0939.

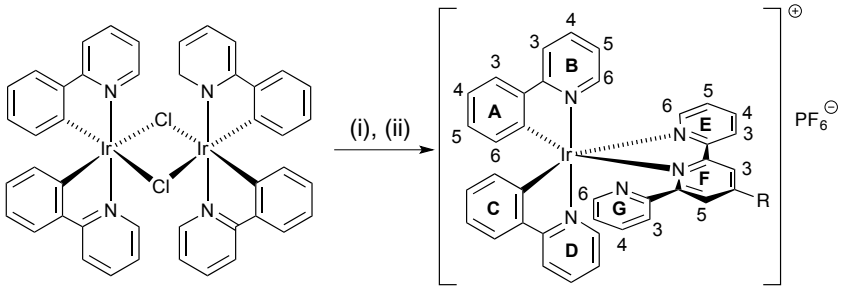

[Ir$_2$(ppy)$_4$Cl$_2$]

[Ir(ppy)$_2$(**1**)][PF$_6$] R = Cl
[Ir(ppy)$_2$(**2**)][PF$_6$] R = OMe
[Ir(ppy)$_2$(**3**)][PF$_6$] R = OEt
[Ir(ppy)$_2$(**4**)][PF$_6$] R = SMe
[Ir(ppy)$_2$(**5**)][PF$_6$] R = SPh
[Ir(ppy)$_2$(**6**)][PF$_6$] R = NMe$_2$

Scheme 2. Synthesis of the [Ir(ppy)$_2$(N^N)][PF$_6$] complexes with atom labelling for NMR spectroscopic assignments. Conditions: (i) N^N, MeOH, microwave reactor, 2 h; (ii) [NH$_4$][PF$_6$].

3 Results and discussion

3.1 Synthesis and NMR spectroscopic characterization

Scheme 2 summarizes the general method for the synthesis of $[Ir(ppy)_2(N^N)][PF_6]$ with N^N = **1**–**6**. The use of the dichlorido dimer is standard methodology for accessing this type of complex, but we have recently reported that traces of chloride salts (see later) may persist [28] and have developed a solvento approach that offers a strategy to chloride-free $[Ir(ppy)_2(N^N)][PF_6]$ complexes [15]. The $[Ir(ppy)_2(N^N)][PF_6]$ complexes were isolated as orange solids in yields of 64–98%. In the electrospray mass spectrum, a base peak corresponding to the $[Ir(ppy)_2(N^N)]^+$ ion was observed for each complex, and the characteristic isotope pattern was consistent with that calculated.

The ^1H and ^{13}C NMR spectra of CD_2Cl_2 solutions of $[Ir(ppy)_2(N^N)][PF_6]$ (N^N = **1**–**6**) were recorded at room temperature. The aromatic regions showed minor variations between the complexes with the exception of (i) the additional phenyl signals in $[Ir(ppy)_2(\mathbf{5})][PF_6]$, and (ii) the response of protons H^{F3} and H^{F5} (see Scheme 2) to the introduction of different 4'-substituents. The ^1H NMR spectrum of $[Ir(ppy)_2(\mathbf{2})][PF_6]$ is shown in Fig. 1 as a representative example. The signals were assigned using COSY, NOESY, HMBC and HMQC techniques. In each complex, the lack of a C_2-axis through the N^N ligand means that the two $[ppy]^-$ ligands are non-equivalent. The two doublets at lowest frequency in the ^1H NMR spectra were assigned to H^{A6} and H^{C6} of the cyclometallated rings. Pairs of protons in the two $[ppy]^-$ ligands were distinguished using cross peaks between H^{A6}, H^{D6} and H^{E6} as well as between H^{B6}, H^{C6} and H^{G6}. The most significant change in the chemical shifts across the series of complexes is observed for protons in the central pyridine ring of the tpy ligand. Signals of H^{F3} and H^{F5} move to higher frequency as the electron withdrawing nature of the substituent increases ($\Delta\delta$ is in the range 1.35 ppm). Rings E and G are affected to a smaller extent and the signals of the cyclometallating ligands show only very marginal changes.

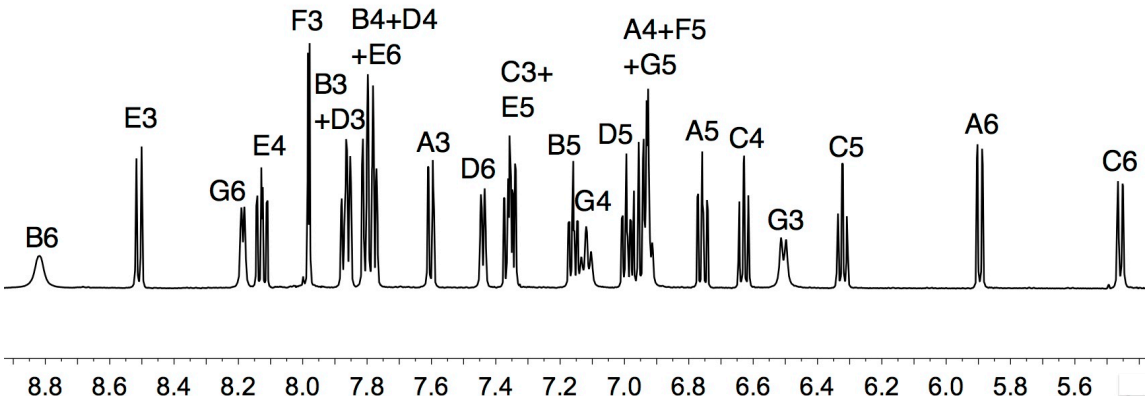

Fig. 1. Aromatic region of the 500 MHz ^{1}H NMR spectrum of [Ir(ppy)$_2$(**2**)][PF$_6$] in CD_2Cl_2 (295 K). Chemical shifts in δ/ppm.

In related complexes containing a 6-phenyl-2,2'-bipyridine as the N^N ligand, the pendant phenyl ring undergoes hindered rotation on the NMR timescale (500 MHz) at room temperature [12, 13, 14, 15] and signals corresponding to the *ortho* and *meta*-protons of the phenyl ring are broad. This dynamic process is retained when the phenyl is replaced by a pyridyl group although (at the same field strength) broadening of the signals for ring G (Scheme 2) is less than for analogous phenyl-substituted complexes [18]. This is associated with an intramolecular CH...N hydrogen bond between the N donor of ring G and proton H^{B6} (see structural discussions), as previously observed for [Ir(ppy)$_2$(tpy)][PF$_6$] [18]. As ring G rotates, proton H^{B6} experiences more than one environment as the CH...N hydrogen bond is sequentially formed and broken. At 298 K, the H^{B6} resonance is broad (FWHM ≈ 16 Hz) and appears at relatively high frequency (δ 8.8–8.9 ppm).

Variable temperature ^{1}H NMR spectra for a CD_2Cl_2 solution of [Ir(ppy)$_2$(**6**)][PF$_6$] are shown in Fig. 2, and reveal two independent dynamic processes which coincidently possess similar activation barriers. On cooling, the collapse of the signal for H^{B6} (δ 8.82 ppm) and growth of the signal at δ 9.02 ppm coupled with

changes in the signals for ring G protons are consistent with freezing out the conformer of $[Ir(ppy)_2(\mathbf{6})]^+$ in which the pendant pyridyl ring is hydrogen-bonded to H^{B6}. The second dynamic process involves the NMe_2 group. At 295 K, the two methyl groups are equivalent (δ 3.19 ppm, Fig. 2) and on cooling, the signal collapses and is resolved as two signals (δ 3.04 and 3.26 ppm) at 210 K. Despite the π-conjugation between the NMe_2 group and the pyridine ring to which it is bonded (see structural discussion), the barrier to rotation at 295 K is relatively low.

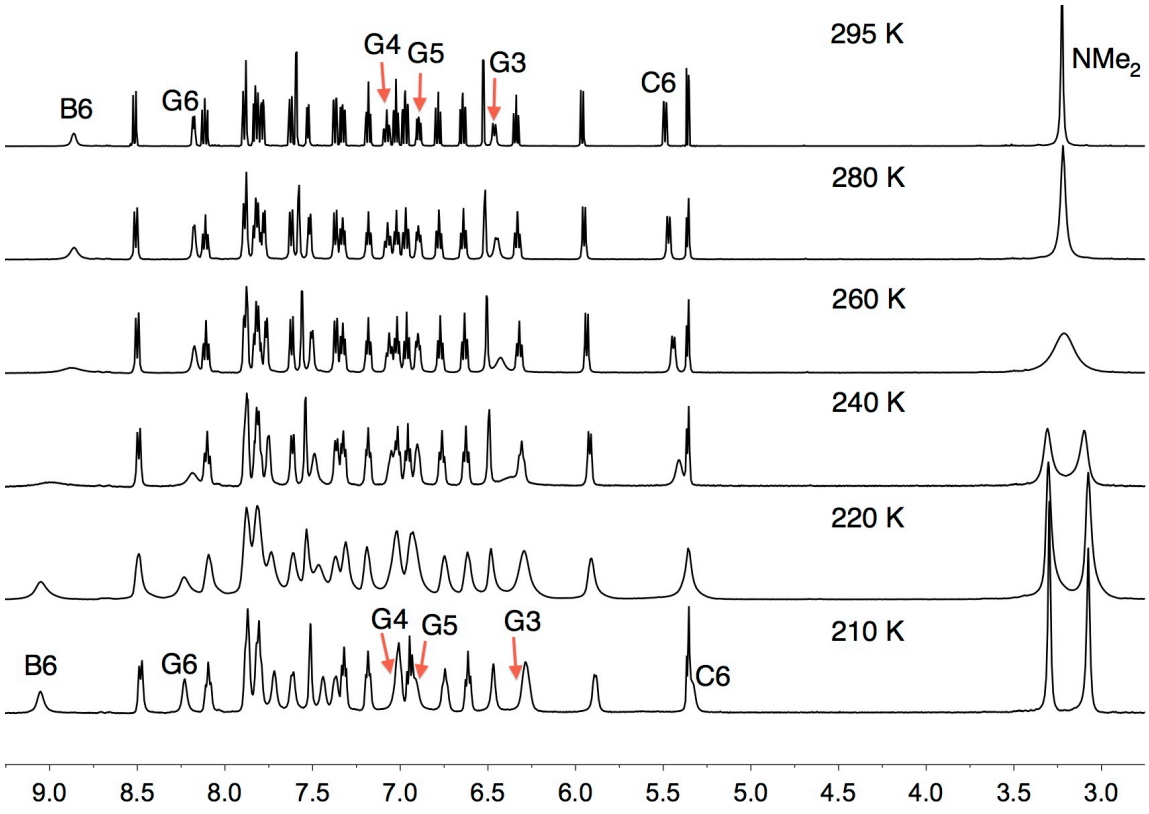

Fig. 2. Variable temperature ^{1}H NMR spectra of $[Ir(ppy)_2(\mathbf{6})][PF_6]$ (500 MHz, CD_2Cl_2).

*3.2 Single crystal structures of 2{[Ir(ppy)$_2$(**1**)][PF$_6$]}·0.6Et$_2$O·CH$_2$Cl$_2$, [Ir(ppy)$_2$(**5**)][PF$_6$]·0.5CH$_2$Cl$_2$ and [Ir(ppy)$_2$(**6**)][PF$_6$]*

Single crystals of $2\{[Ir(ppy)_2(\mathbf{1})][PF_6]\}\cdot 0.6Et_2O\cdot CH_2Cl_2$, $[Ir(ppy)_2(\mathbf{5})][PF_6]\cdot 0.5CH_2Cl_2$ and $[Ir(ppy)_2(\mathbf{6})][PF_6]$ were grown from CH_2Cl_2 solutions of each complex by slow evaporation or Et_2O diffusion. Each complex cation contains a tris-chelated octahedral Ir atom and each compound crystallizes in an achiral space group with both the Δ- and Λ-

$[Ir(ppy)_2(N^N)]^+$ ions in the unit cell. In $2\{[Ir(ppy)_2(\mathbf{1})][PF_6]\}\cdot 0.6Et_2O\cdot CH_2Cl_2$, the asymmetric unit contains two independent $[Ir(ppy)_2(\mathbf{1})]^+$ cations of opposite handedness, one of which is shown in Fig. 3. Bond distances and chelate angles in the coordination sphere of both independent cations are similar and data for one cation are given in the caption to Fig. 3. The asymmetric unit in $[Ir(ppy)_2(\mathbf{5})][PF_6]\cdot 0.5CH_2Cl_2$ also contains two independent complex cations of opposite chirality, and in one, ligand **5** is disordered and has been modelled over two sites of occupancies 0.72 and 0.28. Figure 4 depicts the structure of the ordered $[Ir(ppy)_2(\mathbf{5})]^+$ cation. The coordination spheres in the $[Ir(ppy)_2(\mathbf{5})]^+$ and $[Ir(ppy)_2(\mathbf{6})]^+$ cations exhibit similar structural parameters (see captions to Figs. 4 and 5) to those of $[Ir(ppy)_2(\mathbf{1})]^+$ and offer no surprising details. In view of the dynamic behaviour of the NMe_2 group in $[Ir(ppy)_2(\mathbf{5})][PF_6]$ (see above), it is noteworthy that the group is planar in the solid-state (see bond parameters in Fig. 5 caption) consistent with delocalization of π-electrons into the central pyridine ring of ligand **6**; the N4–C8 bond length of 1.352(3) Å indicates multiple bond character and the torsion angle C7–C8–N4–C16 is 9.0(3)°. In each $[Ir(ppy)_2(N^N)]^+$ cation, the tpy unit is significantly twisted and this is associated with intramolecular π-stacking of the non-coordinated pyridine ring over the phenyl ring of one of the $[ppy]^-$ ligands. The structure of one of the independent $[Ir(ppy)_2(\mathbf{1})]^+$ cations is shown in Fig. 6 as a representative example. Table 1 gives the twist angles between adjacent pairs of pyridine rings in the tpy units in each cation. Parameters that define the face-to-face π-interaction are also given in Table 1, and are quite similar for all complexes, demonstrating efficient π-stacking.

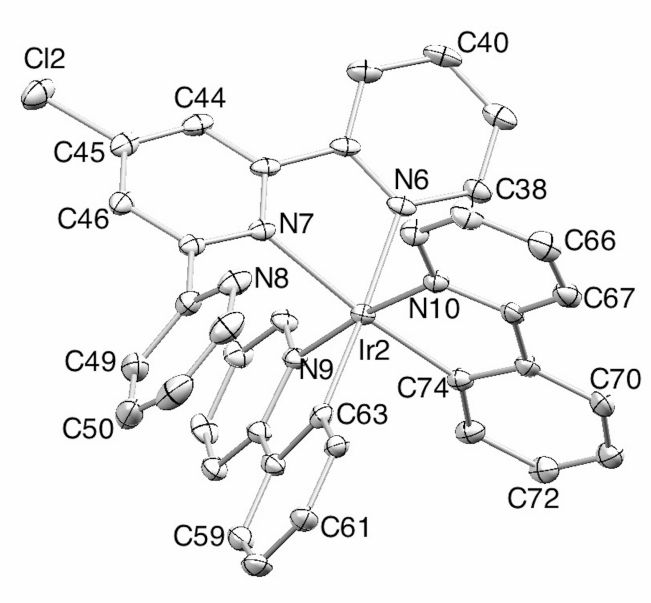

Fig. 3. Structure of one of the independent $[Ir(ppy)_2(\mathbf{1})]^+$ ions in $2\{[Ir(ppy)_2(\mathbf{1})][PF_6]\}\cdot 0.6Et_2O\cdot CH_2Cl_2$; H atoms omitted and ellipsoids plotted at 30% probability. Selected bond parameters: Ir2–N6 = 2.140(4), Ir2–N7 = 2.210(4), Ir2–N9 = 2.052(4), Ir2–N10 = 2.045(4), Ir2–C63 = 2.008(4), Ir2–C74 = 2.007(5), Cl2–C45 = 1.720(5) Å; N6–Ir2–N7 = 76.40(15), N9–Ir2–C63 = 80.19(16), N10–Ir2–C74 = -81.12(18)°.

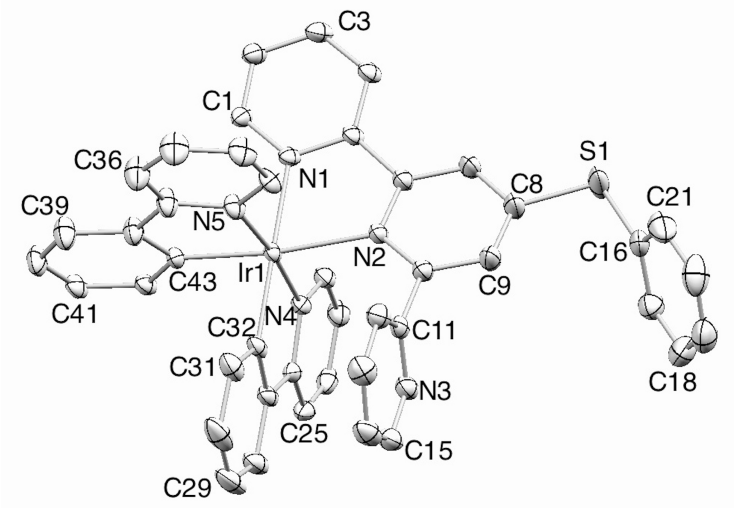

Fig. 4. The structure of one of the independent (ordered) $[Ir(ppy)_2(\mathbf{5})]^+$ cations in $[Ir(ppy)_2(\mathbf{5})][PF_6]\cdot 0.5CH_2Cl_2$; H atoms omitted and ellipsoids plotted at 30% probability. Selected bond parameters: Ir1–N1 = 2.135(3), Ir1–N2 = 2.204(3), Ir1–N4 = 2.044(3), Ir1–N5 = 2.039(3), Ir1–C32 = 2.027(4), Ir1–C43 = 2.011(4), S1–C8 = 1.765(5), S1–C16 = 1.762(5) Å; N1–Ir1–N2 = 76.26(12), N4–Ir1–C32 = 80.19(16), N5–Ir1–C43 = 80.58(15), C8–S1–C16 = 103.3(2)°.

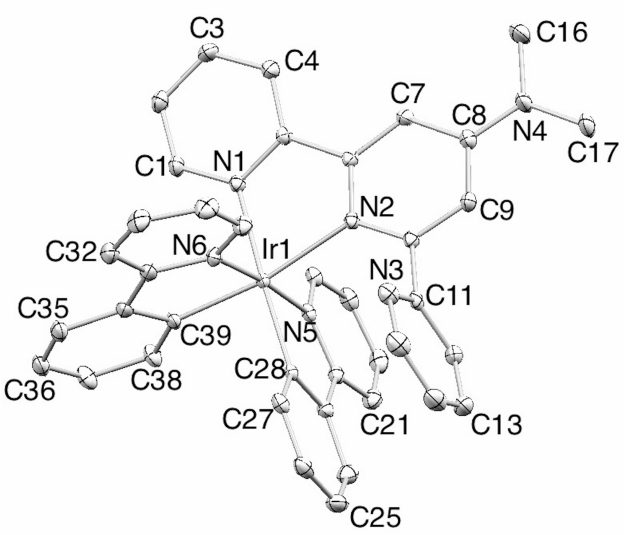

Fig. 5. The structure of the $[Ir(ppy)_2(\mathbf{6})]^+$ cation in $[Ir(ppy)_2(\mathbf{6})][PF_6]$; H atoms omitted and ellipsoids plotted at 40% probability. Selected bond parameters: Ir1–N1 = 2.1377(15), Ir1–N2 = 2.1987(15), Ir1–N5 = 2.0508(14), Ir1–N6 = 2.0403(16), Ir1–C28 = 2.0166(17), Ir1–C39 = 2.0096(19), N4–C8 = 1.352(3), N4–C16 = 1.460(3), N4–C17 = 1.459(3) Å; N1–Ir1–N2 = 76.16(6), N5–Ir1–C28 = 80.08(6), N6–Ir1–C39 = 80.35(7), C8–N4–C16 = 120.78(17), C8–N4–C17 = 120.29(17), C16–N4–C17 = 117.79(17)°.

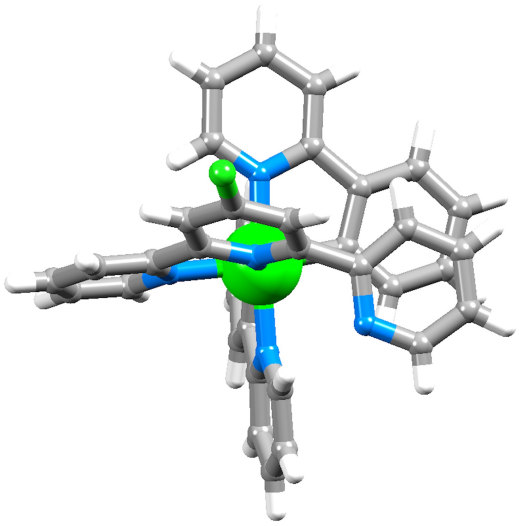

Fig. 6. View of one of the independent $[Ir(ppy)_2(\mathbf{1})]^+$ cations showing the twisted tpy unit and face-to-face π-interaction between the pendant pyridine ring and one cyclometallated ring.

Table 1 Structural parameters that define the deformation of the tpy unit and the face-to-face π-interaction in $[Ir(ppy)_2(N^N)]^+$ cations.

	$[Ir(ppy)_2(\mathbf{1})]^+$ Cation 1	$[Ir(ppy)_2(\mathbf{1})]^+$ Cation 2	$[Ir(ppy)_2(\mathbf{5})]^+$ Cation 1	$[Ir(ppy)_2(\mathbf{5})$ Cation 2	$[Ir(ppy)_2(\mathbf{6})]^+$
Angle between planes of rings with N1/N2 (or N6/N7)[a] / deg	17.2	23.2	13.3	3.8	15.1
Angle between planes of rings with N2/N3 (or N7/N8)[a] / deg	66.0	60.2	81.3	83.8	72.0
Angle between planes of rings with N3/C37 (N8/C68)[a] / deg	6.2	9.2	4.0	8.1	5.6
$Pyridine_{centroid}$ ...$phenyl_{plane}$ distance / Å	3.25	3.22	3.18	3.31	3.21
$Pyridine_{centroid}$ ...$phenyl_{centroid}$ distance / Å	3.55	3.54	3.44	3.41	3.41

[a]See Figs. 3–5 for ring labelling; where there are two independent molecules, the tpy unit contains either N1, N2 and N3, or N6, N7 and N8. For the disordered $[Ir(ppy)_2(\mathbf{5})]^+$ cation, only the major occupancy is considered.

3.3 Single crystal structure of $[Ir(ppy)_2(\mathbf{3})]Cl{\cdot}2H_2O{\cdot}MeCN$

Traces of chloride ion carried through in the synthesis of $[Ir(ppy)_2(\mathbf{3})][PF_6]$ led to the serendipitous growth of X-ray quality crystals of $[Ir(ppy)_2(\mathbf{3})]Cl{\cdot}2H_2O{\cdot}MeCN$. Minor chloride impurities are known to be difficult to irradicate when the direct precursor to the $[Ir(ppy)_2(N^N)][PF_6]$ salt is the chlorido dimer (Scheme 2) [28]. The complex crystallizes in the monoclinic space group $P2_1/c$ with both enantiomers of the $[Ir(ppy)_2(\mathbf{3})]^+$ cation in the unit cell. Fig. 7 shows the structure of the Λ-$[Ir(ppy)_2(\mathbf{3})]^+$ cation in the asymmeric unit; bond lengths and angles (caption to Fig. 7) are unexceptional. The non-coordinated pyridine ring (ring with N3, Fig. 7) lies over the

cyclometallated ring containing C28 giving an efficient π-stacking interaction; the angle between the least squares planes through the rings is 3.3°, and the $phenyl_{centroid}$...$pyridine_{plane}$ separation is 3.24 Å. The packing consists of chloride-water ribbons of stoichiometry $\{(H_2O)_2Cl^-\}_n$ running through channels between chains of octahedral $[Ir(ppy)_2(\mathbf{3})]^+$ cations. Each ribbon consists of edge-sharing hydrogen-bonded pentacycles (Fig. 8), and the assembly complements the wide variety of chloride–water networks and clusters that have previously been reported [29-35]. In each hydrogen-bonded polygon, the independent Cl...O separations are 3.198(3), 3.099(3) and 3.233(3) Å and the O...O distance is 2.742(4) Å.

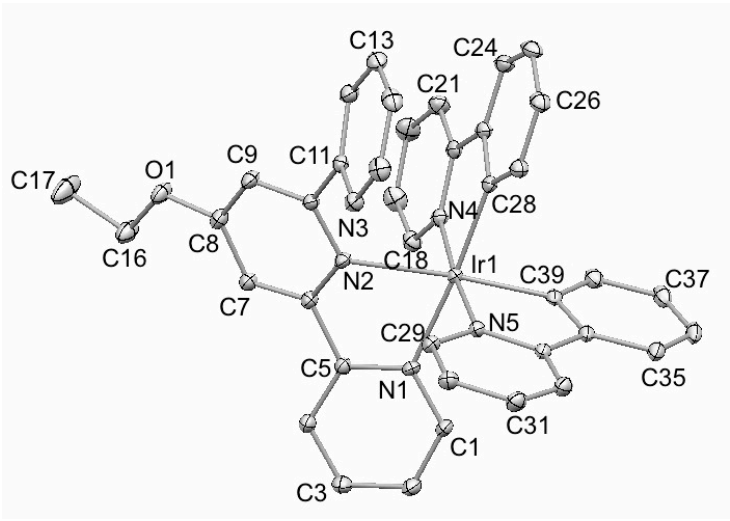

Fig. 7. Structure of the Λ-$[Ir(ppy)_2(\mathbf{3})]^+$ cation in $[Ir(ppy)_2(\mathbf{3})]Cl{\cdot}2H_2O{\cdot}MeCN$. Hydrogen atoms are omitted and ellipsoids are plotted at 40% probability level. Selected bond parameters: Ir1–N1 = 2.136(2), Ir1–N2 = 2.2229(19), Ir1–N4 = 2.0541(19), Ir1–N5 = 2.0424(19), Ir1–C28 = 2.017(2), Ir1–C39 = 2.002(2), O1–C8 = 1.342(3), O1–C16 = 1.449(3) Å; N1–Ir1–N2 = 75.50(7), N4–Ir1–C28 = 80.05(9), N5–Ir1–C39 = 80.31(9), C8–O1–C16 = 118.3(2)°.

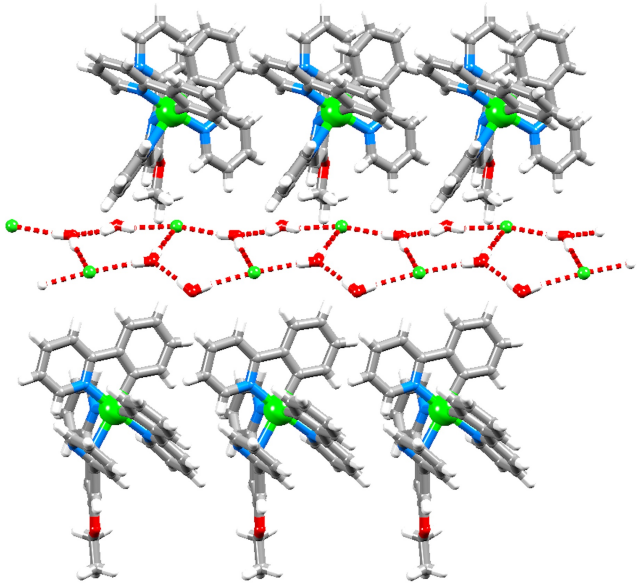

Fig. 8. Chains of cations separated by hydrogen-bonded water–chloride ion chains in [Ir(ppy)$_2$(**3**)]Cl·2H$_2$O·MeCN; the MeCN molecules are omitted.

3.4 Solution electrochemical and photophysical properties

The redox behaviour of the complexes was studied by cyclic voltammetry and square wave voltammetry, and redox potentials are given in Table 2. Data for [Ir(ppy)$_2$(tpy)][PF$_6$] [18] are included in Table 2 for comparison. The electrochemical behaviour of the complexes is similar to that of related complexes previously reported [2,18,36]. Each complex exhibits an irreversible, iridium-centred oxidation. On going from the parent complex [Ir(ppy)$_2$(tpy)]$^+$ to [Ir(ppy)$_2$(**1**)]$^+$, the introduction of the electron-withdrawing chloro-substituent causes a small shift to higher potential for the iridium(III) oxidation. The most noticeable change in oxidation potential (from +0.90 V in [Ir(ppy)$_2$(tpy)][PF$_6$] to +0.81 V in [Ir(ppy)$_2$(**6**)][PF$_6$]) is upon the introduction of the electron-releasing NMe$_2$ group. Within the solvent accessible window, either one or two reduction processes are observed (Table 2). The first reduction is quasi-reversible; it is assigned to a tpy-centred process [18] since the LUMO of [Ir(C^N)$_2$(N^N)]$^+$ complexes is localized on the N^N chelate [1]. Table 2 also shows the electrochemical HOMO–

LUMO gap ($\Delta E_{1/2}$) which can be correlated with the emission maxima as discussed below.

Table 2. Cyclic voltammetric data with respect to Fc/Fc^+; degassed CH_2Cl_2 solutions with $[^nBu_4N][PF_6]$ supporting electrolyte, and scan rate of 0.1 V s^{-1} (ir = irreversible; qr = quasi-reversible).

Complex	$E_{1/2}^{ox}$ / V	$E_{1/2}^{red}$ / V	$\Delta E_{1/2}$ / V
$[Ir(ppy)_2(tpy)][PF_6]$[a]	$+0.90^{ir}$	-1.82^{qr}	2.72
$[Ir(ppy)_2(\mathbf{1})][PF_6]$	$+0.92^{ir}$	-1.71^{qr}, -2.38^{ir}	2.63
$[Ir(ppy)_2(\mathbf{2})][PF_6]$	$+0.86^{ir}$	-1.92^{qr}	2.78
$[Ir(ppy)_2(\mathbf{3})][PF_6]$	$+0.85^{ir}$	-1.93^{qr}	2.78
$[Ir(ppy)_2(\mathbf{4})][PF_6]$	$+0.88^{ir}$	-1.83^{qr}, -2.47^{ir}	2.71
$[Ir(ppy)_2(\mathbf{5})][PF_6]$	$+0.90^{ir}$	-1.75^{qr}, -2.39^{ir}	2.66
$[Ir(ppy)_2(\mathbf{6})][PF_6]$	$+0.81^{ir}$	-2.05^{qr}	2.86

[a]From reference [16].

The solution absorption spectra of the complexes are shown in Fig. 9. All complexes exhibit an intense absorption maximum in the UV region assigned to C^N and N^N ligand based spin-allowed π*←π and π*←n transitions. Absorption bands with the maximum at ≈270 nm are characteristic for $[ppy]^-$-centred (^{1}LC) transitions whereas the absorptions between 280 and 330 nm have larger contributions of ligand centred transitions on the N^N ligand [2,36]. The lower energy absorptions (Fig. 9) are assigned to spin-allowed charge transfer (^{1}MLCT and ^{1}LLCT) transitions [^{1}]. The spectra of $[Ir(ppy)_2(\mathbf{2})][PF_6]$ and $[Ir(ppy)_2(\mathbf{3})][PF_6]$ (both with alkoxy substituents) are essentially the same. Similarly, $[Ir(ppy)_2(\mathbf{4})][PF_6]$ and $[Ir(ppy)_2(\mathbf{5})][PF_6]$ (with SMe and SPh substituents respectively) exhibit similar absorptions, and these are red-shifted with respect to the absorptions of the complexes with alkoxy substituents.

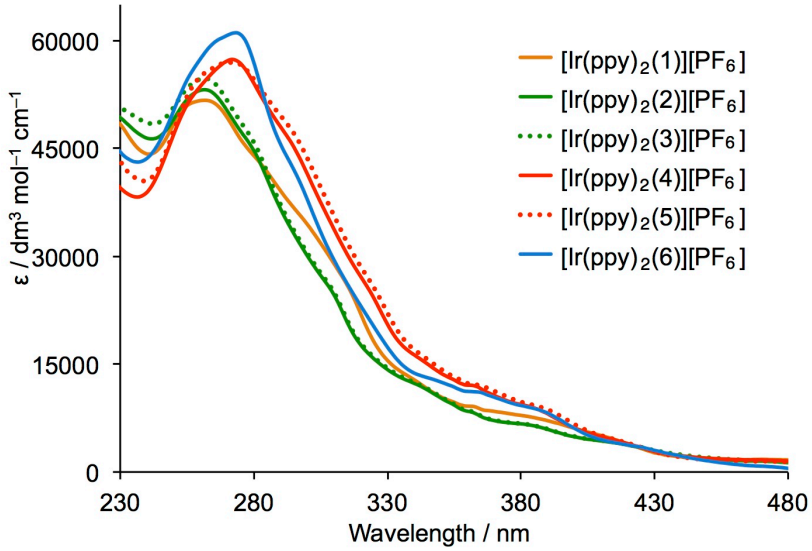

Fig. 9. Solution absorption spectra of the $[Ir(ppy)_2(N^N)][PF_6]$ complexes (CH_2Cl_2, 1.25 × 10^{-5} mol dm^{-3}).

The photoluminescence spectra of degassed CH_2Cl_2 solutions of the cyclometallated iridium complexes are shown in Fig. 10; excitation wavelengths, quantum yields and emission lifetimes are summarized in Table 3. The emitting state of an $[Ir(C^N)_2(N^N)]^+$ complex is the lowest energy triplet state [1], and broad bands as observed in Fig. 10 are characteristic of dominant charge-transfer (^{3}MLCT and ^{3}LLCT) contributions. The emission maxima range from 550 nm for $[Ir(ppy)_2(\mathbf{6})][PF_6]$ (electron-releasing NMe_2 substituent) to 607 nm for $[Ir(ppy)_2(\mathbf{1})][PF_6]$ electron-withdrawing chloro-substituent, and the order of values of λ_{max}^{em} is in agreement with the trend in the electrochemical HOMO–LUMO gaps given in Table 2. The solution photoluminescence quantum yields are <5% for all complexes except $[Ir(ppy)_2(\mathbf{6})][PF_6]$ which performs significantly better than the remaining complexes both in terms of quantum yield and emission lifetime (Table 3).

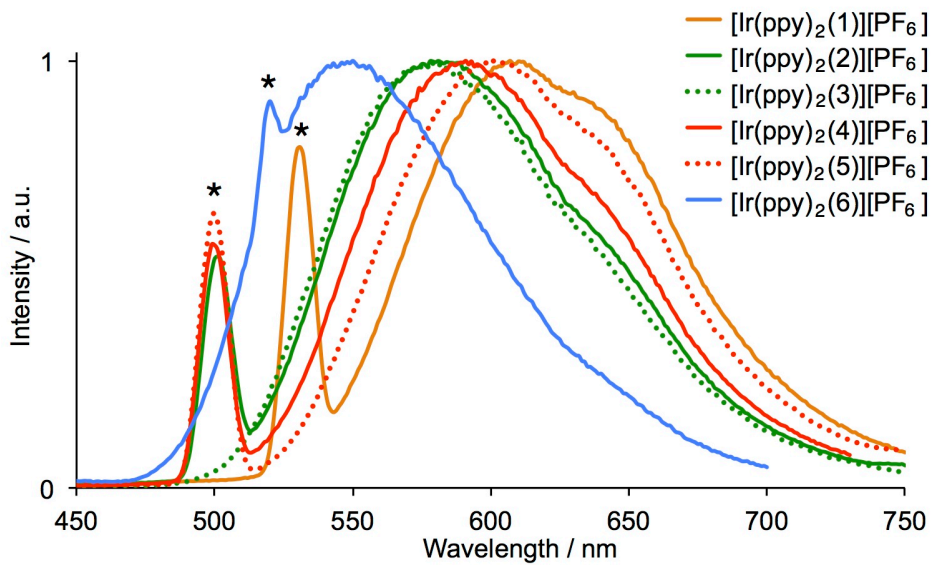

Fig. 10. Normalized emission spectra of degassed CH_2Cl_2 solutions of the $[Ir(ppy)_2(N^N)][PF_6]$ complexes (1.25×10^{-5} mol dm^{-3}). Excitation wavelengths are given in Table 3; * = first harmonic.

Table 3. Emission maxima (λ_{em}^{max}) with excitation wavelengths (λ_{ex}), emission lifetimes ($\tau_{1/2}$) and quantum yields (QY); solutions were degassed.

Complex	λ_{ex} / nm	λ_{em}^{max} / nm	$\tau_{1/2}$ / ns	QY / %
$[Ir(ppy)_2(\mathbf{1})][PF_6]$	265	607	55	2.8
$[Ir(ppy)_2(\mathbf{2})][PF_6]$	250	580	107	4.7
$[Ir(ppy)_2(\mathbf{3})][PF_6]$	250	578	105	4.2
$[Ir(ppy)_2(\mathbf{4})][PF_6]$	250	591	92	4.6
$[Ir(ppy)_2(\mathbf{5})][PF_6]$	250	601	77	3.8
$[Ir(ppy)_2(\mathbf{6})][PF_6]$	260	550	441	24.8

4 Conclusions

We have prepared and characterized a series of cyclometallated iridium(III) complexes $[Ir(ppy)_2(N^N)][PF_6]$ in which the N^N ligand **1**–**6** is a 4'-substituted tpy bearing electron-withdrawing or releasing substituents. The single crystal structures of four representative complexes confirm the expected octahedral coordination sphere of the iridum(III) atom with each tpy ligand coordinating in a bidentate manner; the pendant

pyridine moiety stacks over the phenyl ring of an adjacent cyclometallated $[ppy]^-$ ligand, engaging in an efficient face-to-face π-stacking interaction. Variable temperature solution NMR spectra have been used to probe the dynamics in $[Ir(ppy)_2(\mathbf{6})][PF_6]$; two processes (hindered rotation of the non-coordinated pyridine ringand rotation around the conjugated $C_{pyridine}–N_{NMe_2}$ bond) occur with similar actvation barriers. The single crystal structure of $[Ir(ppy)_2(\mathbf{3})]Cl\cdot 2H_2O\cdot MeCN$ reveals that rows of $[Ir(ppy)_2(\mathbf{3})]^+$ cations are separated by chloride-water ribbons of stoichiometry $\{(H_2O)_2Cl^-\}_n$. Trends in the electrochemical HOMO–LUMO gaps and emission maxima of the complexes are consistent with the electron-withdrawing or releasing properties of the 4'-tpy substituent; in degassed solution, $[Ir(ppy)_2(\mathbf{6})][PF_6]$ has a quantum yield of 24.8% and emission lifetime of 441 ns, while the other complexes exhibit significantly lower quantum yields and shorter lifetimes.

Appendix 1 Supplementary data

Crystallographic data for all the complexes have been deposited with the CCDC (Cambridge Crystallographic Data Centre, 12 Union Road, Cambridge CB2 1EZ, UK; fax +44 1223 336 033; e-mail: deposit@ccdc.cam.ac.uk or www: http://www.ccdc.cam.ac.uk) and may be obtained free of charge on quoting the deposition number CCDC 1405414-1405417.

Acknowledgements

We thank the Swiss National Science Foundation, the University of Basel, and the European Research Council (Advanced Grant 267816 LiLo) for financial support. PD Dr Daniel Häussinger and Roché M. Walliser are thanked for assisting with low temperature NMR spectroscopic measurements.

References

[1] R. D. Costa, E. Ortí, H. J. Bolink, F. Monti, G. Accorsi, N. Armaroli, Angew. Chem. Int. Ed. 51 (2012) 8178.

[2] F. Neve, A. Crispini, S. Campagna, S. Serroni, Inorg. Chem. 38 (1999) 2250.

[3] F. Neve and A. Crispini, Eur. J. Inorg. Chem., 2000, 1039.

[4] M. Lepeltier, T. K.-M. Lee, K. K.-W. Lo, L. Toupet, H. Le Bozec, V. Guerchais, Eur. J. Inorg. Chem. (2005) 110.

[5] J. O. Huh, M. H. Lee, H. Jang, K. Y. Hwang, J. S. Lee, S. H. Kim, Y. Do, Inorg. Chem. 47 (2008) 6566.

[6] H. J. Bolink, E. Coronado, R. D. Costa, E. Ortí, M. Sessolo, S. Graber, K. Doyle, M. Neuburger, C. E Housecroft, E. C. Constable, Adv. Mater. 20 (2008) 3910.

[7] S. Graber, K. Doyle, M. Neuburger, C. E. Housecroft, E. C. Constable, R. D. Costa, E. Ortí, D. Repetto, H. J. Bolink, J. Am. Chem. Soc. 130 (2008) 14944.

[8] R. D. Costa, E. Ortí, H. J. Bolink, S. Graber, C. E. Housecroft, M. Neuburger, S. Schaffner, E. C. Constable, Chem. Commun. (2009) 2029.

[9] R. D. Costa, E. Ortí, H. J. Bolink, S. Graber, C. E. Housecroft, E. C. Constable, Adv. Funct. Mater. 20 (2010) 1511.

[10] R. D. Costa, E. Ortí, H. J. Bolink, S. Graber, C. E. Housecroft, E. C. Constable, J. Am. Chem. Soc. 132 (2010) 5978.

[11] R. D. Costa, E. Ortí, H. J. Bolink, S. Graber, C. E. Housecroft and E. C. Constable, Chem. Commun., 2011, 47, 3207.

[12] A. M. Bünzli, H. J. Bolink, E. C. Constable, C. E. Housecroft, M. Neuburger, A. Pertegás and J. A. Zampese, Eur. J. Inorg. Chem., 2012, 3780.

[13] E. Baranoff, H. J. Bolink, E. C. Constable, M. Delgado, D. Häussinger, C. E. Housecroft, M. K. Nazeeruddin, M. Neuburger, E. Ortí, G. E. Schneider, D. Tordera, R. M. Walliser and J. A. Zampese, Dalton Trans. 42 (2013) 1073.

[14] D. Tordera, A. M. Bünzli, A. Pertegás, J. M. Junquera-Hernández, E. C. Constable, J. A. Zampese, C. E. Housecroft, E. Ortí and H. J. Bolink, Chem. Eur. J. 19 (2013) 8597.

[15] A. M. Bünzli, E. C. Constable, C. E. Housecroft, A. Prescimone, J. A. Zampese, G. Longo, L. Gil-Escrig, A. Pertegás, H. J. Bolink, Chem. Sci. 6 (2015) 2843.

[16] D. Sykes, I. S. Tidmarsh, A. Barbieri, I. V. Sazanovich, J. A. Weinstein, M. D. Ward, Inorg. Chem. 50 (2011) 11323.

[17] D. Sykes , S. C. Parker , I. V. Sazanovich , A. Stephenson , J. A. Weinstein, M. D. Ward, Inorg. Chem. 52 (2013) 10500.

[18] E. C. Constable, C. E. Housecroft, G. E. Schneider, J. A. Zampese, H. J. Bolink, A. Pertegás, C. Roldan-Carmona, Dalton Trans. 43 (2014) 4653.

[19] M. Nonoyama, Bull. Chem. Soc. Jpn. 47 (1974) 767.

[20] E. C. Constable, M. D. Ward, J. Chem. Soc., Dalton Trans. (1990) 1405.

[21] E. C. Constable, K. Harris, C. E. Housecroft, M. Neuburger, J. A. Zampese, CrystEngComm 12 (2010) 2949.

[22] Y. Tao, E. C. Constable, C. E. Housecroft, M. Neuburger, Inorg. Chem. Comm. 20 (2102) 180.

[23] E. C. Constable, A. M. W. C. Thompson, D. A. Tocher, M. A. M. Daniels, New J. Chem. 16 (1992) 855.

[24] Bruker Analytical X-ray Systems, Inc., 2006, APEX2, version 2 User Manual, M86-E01078, Madison, WI.

[25] P. W. Betteridge, J. R. Carruthers, R. I. Cooper, K. Prout and D. J. Watkin, J. Appl. Cryst. 36 (2003) 1487.

[26] I. J. Bruno, J. C. Cole, P. R. Edgington, M. K. Kessler, C. F. Macrae, P. McCabe, J. Pearson, R. Taylor, Acta Crystallogr., Sect. B 58 (2002) 389.

[27] C. F. Macrae, I. J. Bruno, J. A. Chisholm, P. R. Edgington, P. McCabe, E. Pidcock, L. Rodriguez-Monge, R. Taylor, J. van de Streek, P. A. Wood, J. Appl. Cryst., 41 (2008) 466.

[28] G. E. Schneider, H. J. Bolink, E. C. Constable, C. D. Ertl, C. E. Housecroft, A. Pertegás, J. A. Zampese, A. Kanitz, F. Kessler, S. B. Meier, Dalton Trans. 43 (2014) 1961.

[29] B. Dey, S. R. Choudhury, P. Gamez, A. V. Vargiu, A. Robertazzi, C.-Y. Chen, H. M. Lee, A. D. Jana, S. Mukhopadhyay, J. Phys. Chem. A, 113 (2009) 8626 and references therein.

[30] J. S. Casas, M. D. Couce, A. Sánchez, J. Sordo, E. M. Vázquez López, Inorg. Chem. Comm. 30 (2013) 156 and references therein.

[31] A. Pati, J. Athilakshmi, V. Ramkumar and D. K. Chand, CrystEngComm, 16 (2014) 6827 and references therein.

[32] E. C. Constable, G. Zhang, C. E. Housecroft, M. Neuburger, S. Schaffner, CrystEngComm 11 (2009) 1014 and references therein.

[33] R. R. Fernandes, A. M. Kirillov, M. F. C. Guedes da Silva, Z. Ma, J. A. L. da Silva, J. J. R. Fraústo da Silva, A. J. L. Pombeiro, Cryst. Growth Des. 8 (2008) 782 and references therein.

[34] S. Chakraborty, R. Dutta, M. Arunachalam, P. Ghosh, Dalton Trans. 43 (2014) 2061 and references therein.

[35] W. Chen, L.-S. Long, R.-B. Huang, L.-S. Zheng, Cryst. Growth Des. 13 (2013) 2507 and references therein.

[36] F. Neve, M. La Deda, F. Puntoriero, and S. Campagna, Inorg. Chim. Acta 359 (2006) 1666.